Transformation of odor representations in target areas of the olfactory bulb

Emre Yaksi*, Francisca von Saint Paul*, Jörn Niessing, Sebastian T. Bundschuh, Rainer W. Friedrich

---

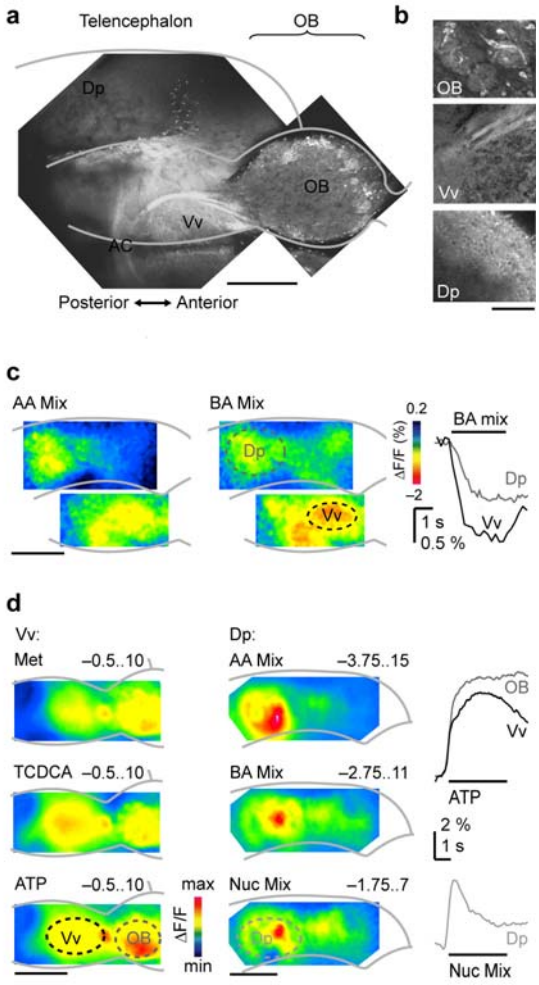

Supplementary Figure 1 Low-resolution mapping of odor-evoked activity in the forebrain. (**a**) Expression of the genetically encoded Ca^{2+} indicator, inverse pericam (IP), under the control of the HuC promoter in the adult zebrafish forebrain (projection of 2-photon stack; ventral view). Scale bar: 200 µm. (**b**) HuC-IP expression in the OB, Vv and Dp at higher resolution. In the OB, IP fluorescence is

Nature Neuroscience: doi:10.1038/nn.2288

observed in somata of MCs and glomerular neuropil. In Vv, fluorescence is observed in axon tracts, but neuronal somata are not fluorescent and appear in negative stain. In Dp, diffuse fluorescence, presumably from projecting MCs, is observed in the background but somata appear negative. Scale bar: 60 µm. (**c**) Wide-field imaging of changes in IP fluorescence in the telencephalon evoked by AA and BA mixtures. Continuous lines outline forebrain contours as in (**a**). Right: time course of IP fluorescence in regions outlined by dashed lines. Bar indicates odor presentation. Decreasing IP fluorescence corresponds to increasing intracellular Ca^{2+} concentration. Responses in the dorsal and ventral telencephalon were measured separately because focal planes differ substantially. Scale bar: 200 µm. (**d**) Wide-field imaging of fluorescence changes evoked by different odor classes in the ventral (left) and dorsal (right) telencephalon after bolus loading of rhod-2-AM. Right: time course of fluorescence changes in regions depicted by dashed lines. Minimum and maximum of the color scale is indicated above each image. Scale bar: 200 µm

To localize odor-responsive areas in the telencephalon, we first measured Ca^{2+} signals using wide-field optics in a transgenic fish line (HuC-IP) that expresses the genetically encoded Ca^{2+} indicator, inverse pericam (IP)[1], in mitral cells of the OB[2]. In the telencephalon, IP fluorescence was observed along the olfactory tracts but not in somata (**a,b**), indicating that IP predominantly or exclusively reports Ca^{2+} signals from projecting axons. Odors with different primary molecular features evoked fluorescence changes in different areas in the OB[2], consistent with the chemotopic organization of glomerular activity patterns[3,4]. In the telencephalon, the same stimuli evoked more widespread fluorescence changes that were most pronounced in the medial telencephalon anterior to the anterior commissure (area Vv) and in the

Nature Neuroscience: doi:10.1038/nn.2288

posterior-lateral telencephalon (area Dp) (**c**; n = 7 fish). In some fish, responses in Dp appeared to consist of two subfields, one slightly anterior to the anterior comissure and the other posterior to the anterior commissure. Vv and Dp both responded to all stimuli in all fish. Within Vv, the distribution of Ca^{2+} signals was widespread and not obviously different in response to AAs and BAs. In Dp, six out of seven fish showed slightly stronger responses to AAs in the posterior part and slightly stronger responses to BAs in the anterior part. However, Ca^{2+} signals evoked by AAs and BAs were always distributed throughout Dp and overlapped substantially.

We next loaded the synthetic Ca^{2+} indicator, rhod-2-AM, into the OB or the telencephalon by bolus injection[5,6]. Consistent with the distribution of Ca^{2+} signals in HuC-IP transgenic fish, changes in rhod-2 fluorescence were most pronounced in Vv and Dp and overlapped substantially in response to different odors (**d**; Vv: n = 7; Dp: n = 12). Within Dp, the posterior part responded more strongly to the AAs and the anterior part responded more strongly to BAs in 10 out of 12 fish, but response patterns were always widespread and overlapping.

These results demonstrate that the differential response of medial and lateral glomeruli to BAs and AAs, respectively, is not mapped onto the medial (Vv) and lateral (Dp) target areas in the telencephalon. One reason for the widespread distribution of odor responses in higher forebrain areas could be non-topographic projections after mitral cell axons exit the OB via the nearest olfactory tract[7]. This hypothesis is supported by the finding that response distributions were similar when a Ca^{2+} indicator was introduced into projecting axons (HuC-IP) or telencephalic neurons (rhod-2-AM). Consistent with this interpretation, anatomical data in other species indicate that many projections to higher olfactory brain areas in vertebrates are divergent[8-10], although they may not be entirely random[11-14]. In addition, activity

Nature Neuroscience: doi:10.1038/nn.2288

downstream of the OB may be distributed by connections between higher-order neurons, both within and across different telencephalic areas[15,16].

1. Nagai, T., Sawano, A., Park, E.S. & Miyawaki, A. Circularly permuted green fluorescent proteins engineered to sense Ca2+. *Proc. Natl. Acad. Sci. USA* **98**, 3197-3202. (2001).
2. Li, J., *et al.* Early development of functional spatial maps in the zebrafish olfactory bulb. *J. Neurosci.* **25**, 5784-5795 (2005).
3. Friedrich, R.W. & Korsching, S.I. Combinatorial and chemotopic odorant coding in the zebrafish olfactory bulb visualized by optical imaging. *Neuron* **18**, 737-752 (1997).
4. Friedrich, R.W. & Korsching, S.I. Chemotopic, combinatorial and noncombinatorial odorant representations in the olfactory bulb revealed using a voltage-sensitive axon tracer. *J. Neurosci.* **18**, 9977-9988 (1998).
5. Stosiek, C., Garaschuk, O., Holthoff, K. & Konnerth, A. In vivo two-photon calcium imaging of neuronal networks. *Proc Natl Acad Sci U S A* **100**, 7319-7324 (2003).
6. Yaksi, E. & Friedrich, R.W. Reconstruction of firing rate changes across neuronal populations by temporally deconvolved Ca^{2+} imaging. *Nat. Methods* **3**, 377-383 (2006).
7. Fuller, C.L., Yettaw, H.K. & Byrd, C.A. Mitral cells in the olfactory bulb of adult zebrafish (Danio rerio): Morphology and distribution. *J. Comp. Neurol.* **499**, 218-230 (2006).
8. Haberly, L.B. Neuronal circuitry in olfactory cortex: anatomy and functional implications. *Chem. Senses* **10**, 219-238 (1985).
9. Finger, T.E. The distribution of the olfactory tracts in the bullhead catfish, Ictalurus nebulosus. *J. Comp. Neurol.* **161**, 125-141 (1975).
10. von Bartheld, C.S., Meyer, D.L., Fiebig, E. & Ebbesson, S.O. Central connections of the olfactory bulb in the goldfish, Carassius auratus. *Cell Tissue Res.* **238**, 475-487 (1984).
11. Ojima, H., Mori, K. & Kishi, K. The trajectory of mitral cell axons in the rabbit olfactory cortex revealed by intracellular HRP injection. *J. Comp. Neurol.* **230**, 77-87 (1984).
12. Buonviso, N., Revial, M.F. & Jourdan, F. The Projections of Mitral Cells from Small Local Regions of the Olfactory Bulb: An Anterograde Tracing Study Using PHA-L (Phaseolus vulgaris Leucoagglutinin). *Eur. J. Neurosci.* **3**, 493-500 (1991).
13. Scott, J.W., McBride, R.L. & Schneider, S.P. The organization of projections from the olfactory bulb to the piriform cortex and olfactory tubercle in the rat. *J. Comp. Neurol.* **194**, 519-534 (1980).
14. Haberly, L.B. & Price, J.L. The axonal projection patterns of the mitral and tufted cells of the olfactory bulb in the rat. *Brain Res.* **129**, 152-157 (1977).
15. Haberly, L.B. Parallel-distributed processing in olfactory cortex: new insights from morphological and physiological analysis of neuronal circuitry. *Chem. Senses* **26**, 551-576. (2001).

Nature Neuroscience: doi:10.1038/nn.2288

16. Johnson, D.M., Illig, K.R., Behan, M. & Haberly, L.B. New features of connectivity in piriform cortex visualized by intracellular injection of pyramidal cells suggest that "primary" olfactory cortex functions like "association" cortex in other sensory systems. *J. Neurosci.* **20**, 6974-6982 (2000).

Nature Neuroscience: doi:10.1038/nn.2288

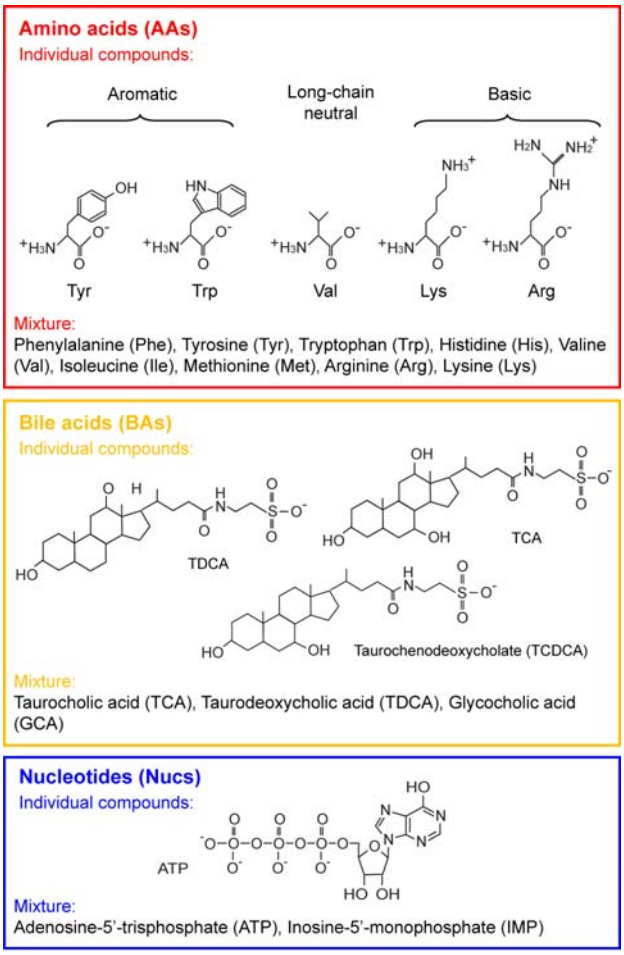

Supplementary Figure 2 Odor stimuli, sorted by molecular features. Structures are shown for stimuli applied as individual compounds; compositions of mixtures used are given below. Concentrations were usually 10 μM for AAs and Nucs and 1 μM for BAs. These concentrations are in the intermediate physiological range[1], do not saturate glomerular responses[2, 3], and have been used in previous experiments. AAs and BAs evoke responses of similar magnitude at these concentrations. In seven experiments, 10-fold higher stimulus concentrations were used, but no obvious differences were observed. Data were therefore pooled.

Nature Neuroscience: doi:10.1038/nn.2288

1. Carr, W.E.S. The molecular nature of chemical stimuli in the aquatic environment. in *Sensory biology of aquatic animals* (ed. J. Atema, R.R. Fay, A.N. Popper & W.N. Tavolga) 3-27 (Springer, New York, 1988).
2. Friedrich, R.W. & Korsching, S.I. Combinatorial and chemotopic odorant coding in the zebrafish olfactory bulb visualized by optical imaging. *Neuron* **18**, 737-752 (1997).
3. Friedrich, R.W. & Korsching, S.I. Chemotopic, combinatorial and noncombinatorial odorant representations in the olfactory bulb revealed using a voltage-sensitive axon tracer. *J. Neurosci.* **18**, 9977-9988 (1998).

Nature Neuroscience: doi:10.1038/nn.2288

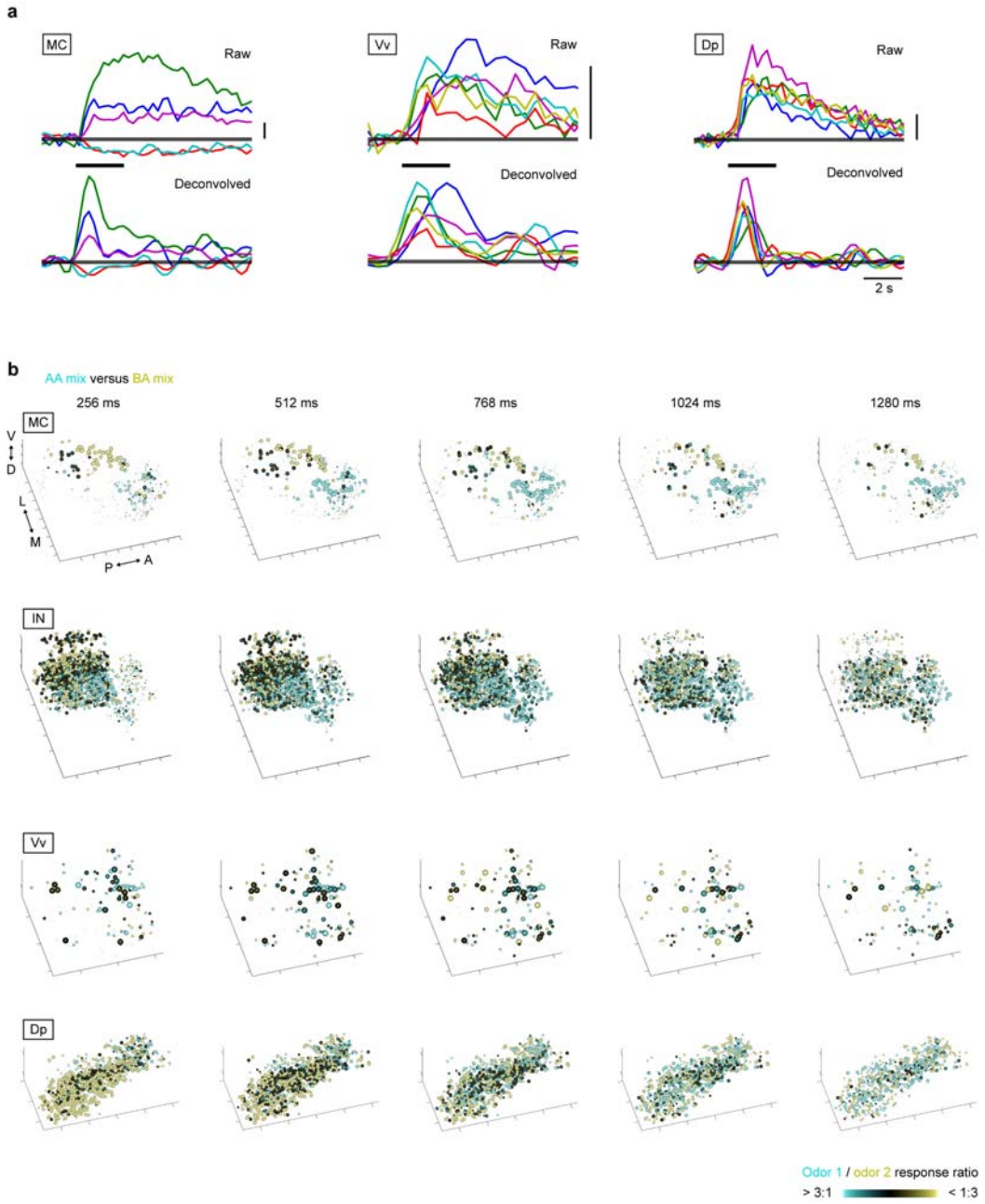

Supplementary Figure 3 Time course of odor responses in different forebrain areas. (**a**) Top: odor-evoked Ca^{2+} signals of five individual MCs (left), six individual Vv neurons (center) and six individual Dp neurons (right). Neurons in each panel were imaged simultaneously. Black bar indicates odor stimulation. Bottom: Temporally deconvolved Ca^{2+} signals. Temporal deconvolution reconstructs firing rate changes and was performed as described using a time constant of 3 seconds[1]. (**b**) Three-

Nature Neuroscience: doi:10.1038/nn.2288

dimensional patterns of deconvolved Ca^{2+} signals at different times after stimulus onset (overlays of responses to AA mixture and BA mixture; same data and conventions as in **Figs. 2** and **3**). Although activity patterns are dynamic, the spatial segregation of AA-responsive and BA-responsive MCs and the lack of an obvious topographic segregation in higher brain areas are apparent throughout the odor response.

1. Yaksi, E. & Friedrich, R.W. Reconstruction of firing rate changes across neuronal populations by temporally deconvolved Ca^{2+} imaging. *Nat. Methods* **3**, 377-383 (2006).

Nature Neuroscience: doi:10.1038/nn.2288

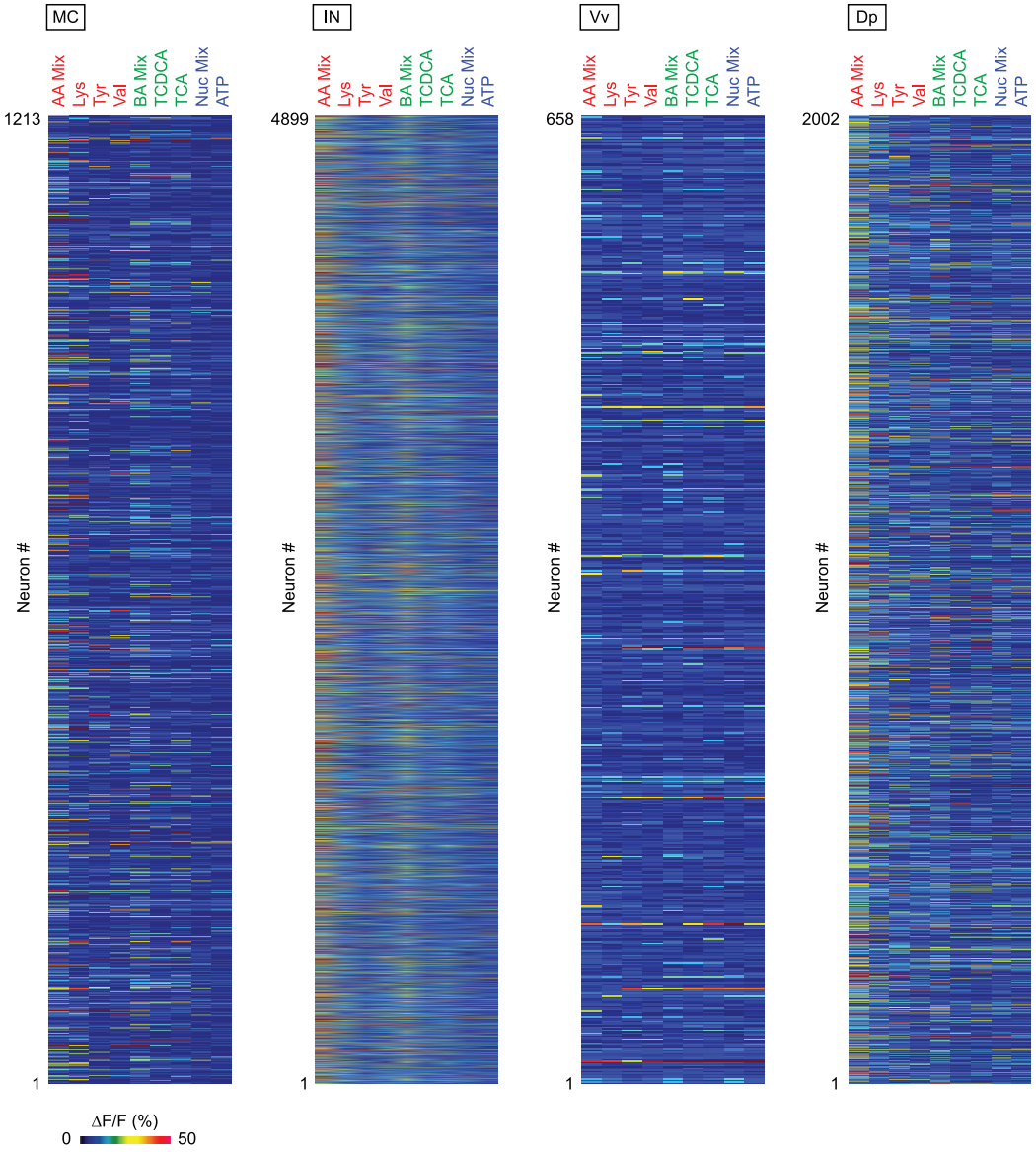

Supplementary Figure 4 Ca^{2+} signals evoked by the nine different stimuli in all MCs (n = 1213), INs (n = 4899), Vv neurons (n = 658) and Dp neurons (n = 2002).

Nature Neuroscience: doi:10.1038/nn.2288

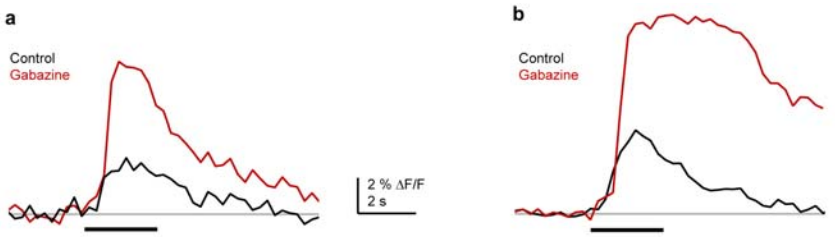

Supplementary Figure 5 Effects of Gabazine on the time course of odor responses in Dp. (**a**) Time course of odor-evoked Ca^{2+} signal before and during application of Gabazine for the experiment shown in **Fig. 6a**, averaged over the entire field of view. (**b**) Time course of spatially averaged Ca^{2+} signal before and during application of Gabazine in another experiment. Focal application of Gabazine increased the magnitude of odor responses in Dp in all experiments (n = 4) and changed the time course. In some experiments, Gabazine slighly prolonged the response (**a**), while in others, Gabazine converted a transient response into a more sustained response (**b**).

Nature Neuroscience: doi:10.1038/nn.2288

Transformation of odor representations in target areas of the olfactory bulb

Emre Yaksi*, Francisca von Saint Paul*, Jörn Niessing, Sebastian T. Bundschuh, Rainer W. Friedrich

---

Supplementary Methods

Animals, dye loading and odor stimulation. Data were collected from 71 adult zebrafish (Danio rerio). Experiments were performed in an explant of the intact brain and nose as described[1]. Briefly, zebrafish were cold-anaesthetized, decapitated, and the ventral forebrain was exposed. The preparation was then placed upside down in a flow chamber, continuously superfused with artificial cerebrospinal fluid (ACSF) for teleosts[2], and warmed up to room temperature. Odors were delivered through a constant flow directed at the nares using a computer-controlled, pneumatically actuated HPLC injection valve (Rheodyne, Rohnert Park, CA). Odor stimuli were of the highest available purity (Fluka, Neu-Ulm, Germany or Sigma Aldrich, Munich, Germany) and applied in a pseudo-random sequence.

Dye loading of OB neurons was performed as described[3,4]. To load telencephalic neurons, the dura mater was removed and 2 – 3 brief (< 1 min) injections were placed within the target area. Measurements started 30 – 60 min after termination of the dye loading procedure. Results obtained with rhod-2-AM and Oregon Green 488 BAPTA-1-AM were not obviously different and pooled.

Imaging and electrophysiology. An overview of the zebrafish forebrain was obtained using confocal reflection microscopy (n = 2 fish). This technique uses a

Nature Neuroscience: doi:10.1038/nn.2288

partially reflecting mirror in a confocal microscope to generate stacks of reflected light images, each of which is a thin optical section as in confocal fluorescence microscopy. Maximum projections of these stacks yield reflected-light images from large fields of view with high resolution and depth of focus. Strongly reflecting structures such as myelinated axon bundles appear bright. Stacks of images were acquired using a LEICA TCS SP2 confocal microscope and software, a 10 x water immersion objective (NA, 0.3), and a 633 nm HeNe laser.

Odor-evoked Ca^{2+} signals were measured by widefield or multiphoton fluorescence microscopy using a custom-made upright microscope[5]. In the widefield mode, fluorescence was excited through an excitation filter (495/30) by a stabilized 150 W Xe arc lamp attenuated to 1.5 – 6% of the full intensity. Fluorescence emission was projected through a dichroic mirror (520 nm long-pass) and an emission filter (545/50) onto the chip of a sensitive CCD camera (CoolSnapHQ; Photometrics, Tucson, AZ). Images were digitized at 12 bits and 5 – 10 Hz. At least two trials were averaged for each stimulus. Two-photon fluorescence was excited by a mode-locked Ti:Sapphire laser (100 fs; 76 or 80 MHz; 800 – 860 nm; Coherent, Santa Clara, CA or SpectraPhysics, Mountain View, CA). Fluorescence emission was detected externally by a photomultiplier-based whole-field detector through emission filters (515/30 for YC and IP; 535/50 for Oregon Green 488 BAPTA-1; 610/75 for rhod-2). Laser intensity was adjusted to minimize photobleaching in each focal plane. Images were acquired at 2 – 8 Hz.

Image acquisition was controlled using CFNT (written by R. Stepnoski of Bell Labs and M. Müller of the Max Planck Institute for Medical Research) or SCANIMAGE (http://svobodalab.cshl.edu)[6]. Image analysis was performed using

Nature Neuroscience: doi:10.1038/nn.2288

custom software written in IgorPro (Wavemetrics, Lake Oswego, OR) or Matlab (Mathworks, Natick, MA).

For topological analyses, odor responses were collected in multiple (up to 30; typically 7 – 12) fields of view in each brain area. The z-distance between fields of view overlapping in x and y was > 15 μm. In the OB, odor responses for 3-D reconstructions were measured in single trials to maximize the number of neurons that were recorded in each experiment. Previous results demonstrated that responses of MCs and INs are highly reproducible[4]. In telencephalic areas and in all mixture experiments, 2 – 4 trials were averaged for each odor stimulus.

Analysis of imaging data. Series of fluorescence images were converted into image series depicting the relative change in fluorescence (ΔF/F) in each pixel. The baseline fluorescence F was determined by averaging raw images over two seconds before stimulus onset. Response maps were constructed by averaging ΔF/F frames over a period of ~3 seconds after response onset. Data obtained with inverse pericam were corrected for bleaching by subtracting ΔF/F series acquired without stimulation. Data obtained with rhod-2 or Oregon Green 488 BAPTA-1 were not corrected because bleaching was minimal.

In 2-photon ΔF/F images, neuronal somata were outlined manually and the response of each soma to each stimulus was determined. Neurons that did not respond to any stimulus were excluded from further analyses. In experiments using binary mixtures, a control analysis demonstrated that mixture interactions did not depend on the sequence of stimulus application, confirming that the observed effects cannot be explained by non-stationary responses. Sparseness was calculated as described previously[7].

Nature Neuroscience: doi:10.1038/nn.2288

Statistical comparisons. A Chi-square test was used to compare proportions. For pairwise comparisons, a non-parametric Wilcoxon rank-sum test was used that does not require normal distributions. No correction for multiple comparisons was performed to minimize the occurrence of false negatives (type 2 errors). This appears more important than minimizing the occurrence of false positives (type 1 errors) because the focus of the analysis is on each pairwise comparison, rather than the total number of significant differences.

Chemotopy index. The calculation of the chemotopy index described in the main text, CI (**Fig. 4b**), is based on the rationale that chemotopic maps have to fulfill two criteria. First, stimuli representing different molecular features should excite distinct sets of neurons. The evoked activity patterns should therefore exhibit low correlation. Second, neurons responding to different molecular features should be spatially segregated. As a consequence, local averaging of activity should not dramatically change the correlation between activity patterns representing different molecular features because response properties of nearby neurons are similar. If neurons are not arranged chemotopically, however, local averaging of responses should increase pattern overlap because responses become, on average, more alike. The correlation of locally averaged activity patterns evoked by odors representing different molecular features will therefore be low if patterns are chemotopic and high if patterns lack chemotopy. To calculate CI, Ca^{2+} signals of neurons were locally averaged using an exponentially decaying weight function (space constant: 50 μm; cutoff at 100 μm). The correlation between activity patterns was then calculated by:

$$r = (1 / n) \Sigma_{i = 1..n} ((X1_i / SD_1) (X2_i / SD_2))$$

Nature Neuroscience: doi:10.1038/nn.2288

where n is the number of neurons, X1 and X2 describe the responses of n neurons to odors 1 and 2, respectively, and SD_1 and SD_2 are the standard deviations of X1 and X2, respectively. Note that unlike in the Pearson correlation coefficient, the mean is not subtracted from X1 and X2 because mean subtraction would remove information about global pattern overlap. CI was then calculated by averaging over the reciprocals of the correlation coefficients:

$$CI = (1 / op) \Sigma_{1..op} r_i^{-1}$$

op is the number of odor pairs and r_i is the correlation between patterns evoked by the i^{th} odor pair, as calculated above. The reciprocal of r was used in order to associate high values of CI with high chemotopy and low values of CI with low chemotopy.

In order to confirm the robustness of the results obtained with CI (**Fig. 4b**), we quantified chemotopy using two additional chemotopy indices, CI2 and CI3. CI2 is identical to CI except that the Pearson correlation coefficient was used as a correlation measure. Because the Pearson correlation coefficient includes the subtraction of the mean activity in each pattern, global pattern overlap contributes less to the chemotopy index in CI2 than in CI. As observed for CI, CI2 was highest for MCs (CI2 = 4.2 ± 14.6; mean ± SD) and significantly different from CI2 for responses of all other cell types (IN: 1.4 ± 13.5; Vv: 1.2 ± 0.1; Dp: 2.1 ± 2.6; $P < 0.005$ for all comparisons; Wilcoxon rank-sum test).

CI3 is based on a similar rationale as CI and CI2 but calculated differently. In each activity pattern, neurons were binned into isotropic voxels with an edge length of 6.4 μm (other values gave similar results). For each voxel and odor, an activity value was calculated by averaging the Ca^{2+} signals of the enclosed somata. Because the dimensions of voxels were small, spatial binning alone did not noticably change the pattern correlation compared to the patterns at single cell resolution. Binned activity

Nature Neuroscience: doi:10.1038/nn.2288

patterns were then locally averaged by convolution with a 3-dimensional Gaussian kernel (sigma = 62 μm; cutoff at 95 μm; other values gave similar results). Examples of the resulting "volume activity maps" are shown as thresholded surface contours in **Fig 2c**. CI3 was then defined as $CI3_{A,B} = 1 - r_{A,B}$, where $r_{A,B}$ is the Pearson correlation coefficient of locally averaged activity patterns evoked by stimuli A and B. CI3 therefore differs from CI because the spatial averaging procedure is different, the mean is subtracted from each pattern, and the difference from one, rather than the reciprocal, is taken. Nevertheless, results were similar to those obtained with CI and CI2: CI3 of MC activity patterns (0.55 ± 0.14; mean ± SD) was significantly higher than CI3 of activity patterns across all other neuron populations (IN: 0.21 ± 0.05; Vv: 0.19 ± 0.05; Dp: 0.30 ± 0.09; $P > 0.005$ for all comparisons; Wilcoxon rank-sum test). All chemotopy indices produced the same rank order of chemotopy (MC > Dp > IN > Vv) and indicate that the chemotopy of MC activity patterns is significantly higher than in all other populations. Hence, CI2 and CI3 confirm the results obtained with CI (**Fig. 4b**).

Further data analysis. CV_{rep} is the mean coefficient of variation determined from two repeated applications of the same odor stimulus. Repeated stimulus applications were separated in time by approximately 40 min. Only neurons with a mean response exceeding at least three times the detection threshold were included, as in other analyses. For the calculation of mixture suppression and synergism, absolute response values were used if both component responses were negative.

1. Tabor, R., Yaksi, E., Weislogel, J.M. & Friedrich, R.W. Processing of odor mixtures in the zebrafish olfactory bulb. *J. Neurosci.* **24**, 6611-6620 (2004).

Nature Neuroscience: doi:10.1038/nn.2288

2. Mathieson, W.B. & Maler, L. Morphological and electrophysiological properties of a novel in vitro preparation: the electrosenspry lateral line lobe brain slice. *J. Comp. Physiol. A* **163**, 489-506 (1988).
3. Yaksi, E. & Friedrich, R.W. Reconstruction of firing rate changes across neuronal populations by temporally deconvolved Ca^{2+} imaging. *Nat. Methods* **3**, 377-383 (2006).
4. Yaksi, E., Judkewitz, B. & Friedrich, R.W. Topological Reorganization of Odor Representations in the Olfactory Bulb. *PLoS Biol.* **5**, e178 (2007).
5. Wachowiak, M., Denk, W. & Friedrich, R.W. Functional organization of sensory input to the olfactory bulb glomerulus analyzed by two-photon calcium imaging. *Proc. Natl. Acad. Sci. USA* **101**, 9097-9102 (2004).
6. Pologruto, T.A., Sabatini, B.L. & Svoboda, K. ScanImage: flexible software for operating laser scanning microscopes. *BioMed. Eng. OnLine* **2**, 13 (2003).
7. Vinje, W.E. & Gallant, J.L. Sparse coding and decorrelation in primary visual cortex during natural vision. *Science* **287**, 1273-1276 (2000).

Nature Neuroscience: doi:10.1038/nn.2288